

Effects of second phases on fracture behavior of Mg-10Gd-3Y-0.6Zr alloy

LIN Dan(林丹)¹, WANG Lei(王磊)¹, MENG Fan-qiang(孟凡强)¹, CUI Jian-zhong(崔建忠)², LE Qi-chi(乐启炽)²

1. Key Laboratory for Anisotropy and Texture of Materials, Ministry of Education,
Northeastern University, Shenyang 110004, China;

2. Key Laboratory of Electromagnetic Processing of Materials, Ministry of Education,
Northeastern University, Shenyang 110004, China

Received 23 September 2009; accepted 30 January 2010

Abstract: The effects of second phases on the fracture behavior of Mg-10Gd-3Y-0.6Zr alloy were investigated. The results show that the fracture mode can be generally described as ductile transgranular fracture in as-extruded condition and intergranular fracture in peak-aged condition. In as-extruded condition, the ductile transgranular fracture occurs by the formation and transgranular propagation of the microcrack from the broken primary phases. However, as the collaboration effects of precipitates inside grains and on the grain boundaries have the tendency to reduce the cohesive strength of the grain boundary, and make the grain boundaries the favorable path for crack propagation, the intergranular fracture occurs in peak-aged condition.

Key words: Mg-Gd-Y-Zr alloy; second phases; microstructure; fracture; tensile properties

1 Introduction

Lightweight magnesium alloys have attracted increasing interest in recent years for potential application in the aerospace, aircraft and racing automotive industries due to their high specific strength[1]. However, because of their HCP structure, the ductility is relatively poor. In order to achieve substantial applications, it is necessary to develop wrought magnesium alloys such as rolled sheets, extruded bar, and forgings[2]. In the past two decades, considerable works have been done to further enhance the strength of wrought Mg alloys through alloying with a combination of two or more kinds of RE elements, which leads to the successful design of Mg-Y-Nd base WE alloys[3]. Recently, magnesium alloys containing gadolinium (Gd) and yttrium (Y) were found to exhibit higher strength than the conventional WE type magnesium alloys at high temperature[4–9]. As the strength of Mg-Gd-Y-Zr alloy is achieved essentially via precipitation strengthening, great efforts have been devoted to analyze the precipitate phases in the matrix. For example, HE et al[10] and WANG et al[11] reported the precipitation sequence of

as-cast Mg-Gd-Y-Zr alloys according to the hardness response to isothermal aging at 523 K for 0–2 400 h.

As the fracture behavior determines the fracture strength and elongation, it is important to understand the relationship between microstructure and mechanical properties[12]. It is well known that the fracture behavior of precipitation-hardening aluminum alloys is essentially dependent on the precipitate phases[13]. But for the precipitation-hardening Mg-Gd-Y-Zr alloy, the relationship between microstructure and fracture behavior has not been clear[14]. Therefore, the fracture behavior of extruded Mg-10Gd-3Y-0.6Zr alloy with and without aging treatment was studied in this work, and the relationship between fracture behavior and second phases was discussed in details.

2 Experimental

An alloy ingot with a nominal composition of Mg-10Gd-3Y-0.6Zr (mass fraction, %) was prepared from high purity Mg (99.95%), Mg-25Gd (mass fraction, %), Mg-25Y (mass fraction, %) and Mg-30Zr (mass fraction, %) master alloys in an electric resistance furnace under the mixed atmosphere of CO₂ and SF₆.

During the process, low-frequency electromagnetic casting (LFEC) technique was used. The actual chemical composition of the alloy was determined to be Mg-10.80Gd-3.03Y-0.61Zr (mass fraction, %). The ingot was homogenized at 773 K for 8 h, and primarily extruded at 703 K with an extruded ratio of 11:1, and then extruded at 653 K with an extruded ratio of 15:1. The extruded alloys were isothermally aged at 498 K for 12 h (T5 heat treatment).

Hardness measurement was carried out on a 450SVD™ Vickers hardness tester with 49 N load and holding time of 15 s. Tensile testing was carried out on a MTS810 type testing machine with a crosshead speed of 0.5 mm/min. The tensile specimens were of bar type with a gauge diameter of 6 mm and a gauge length of 35 mm. The phases were examined by X-ray diffractometer (XRD, Pw3040/60X). Microstructure examination was performed by optical microscope (OM, OLYMPUS GX71), scanning electron microscope (SEM, JSM-7001F) and transmission electron microscope (TEM, TECNAI G²) operating at 200 kV. The TEM specimens were prepared by electrolytic double-jet thinning in a solution of 1% (volume fraction) perchloric acid in alcohol.

3 Results

3.1 Microstructure

The XRD pattern and microstructures of as-extruded alloy are shown in Fig.1. As shown in Fig.1(a), the alloy mainly consists of α -Mg solid solution, $Mg_{24}(Gd,Y)_5$ components and a small amount of $Mg_5(Gd,Y)$ components. The average grain diameter of the alloy is about 10 μm and there are lots of small particles distributing in the matrix (Fig.1(b)). The SEM morphology (Fig.1(c)) indicates that the small particles shown in Fig.1(b) are the regular quadrate-like particles with stoichiometric ratio of Mg to Gd(Y) nearly 24:5, which is consistent with XRD result.

The microstructure and XRD pattern of tested alloy aged at 498 K for 12 h are shown in Fig.2. It can be seen from Fig.2(a) that the average grain diameter is about 10 μm . However, the appearance of precipitates cannot be distinguished by optical microscope. The XRD pattern (Fig.2(b)) indicates that there are lots of $Mg_5(Gd,Y)$ diffraction peaks in T5-treated condition.

3.2 Tensile properties

The tensile properties of the alloy in both as-extruded and aged (498 K for 12 h) conditions are shown in Fig.3. It can be seen that both UTS and YS are improved with aging treatment by 122 and 92 MPa,

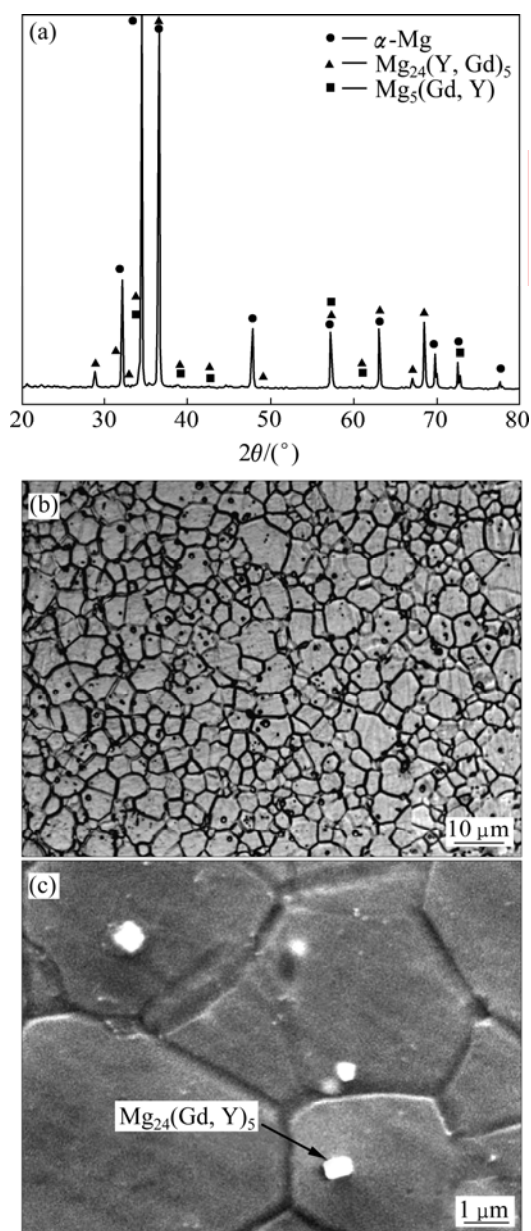


Fig.1 XRD pattern(a), optical morphology(b) and SEM morphology(c) of as-extruded alloy

respectively; while the elongation is decreased.

3.3 Fractography

The typical fracture features of tested alloy are shown in Fig.4. In as-extruded condition, the dimples and broken particles exhibit on fracture surface, as shown in Fig.4(a); and the ductile transgranular fracture features can be seen clearly from Fig.4(b).

After being peak-aged at 489 K, the fracture surface is mainly characterized by grain boundaries, as shown in Fig.4(c), and in some areas, the secondary cracks propagate along the grain boundaries. From Fig.4(d), it can be also noticed that the intergranular fracture occurs in local area for aged alloy.

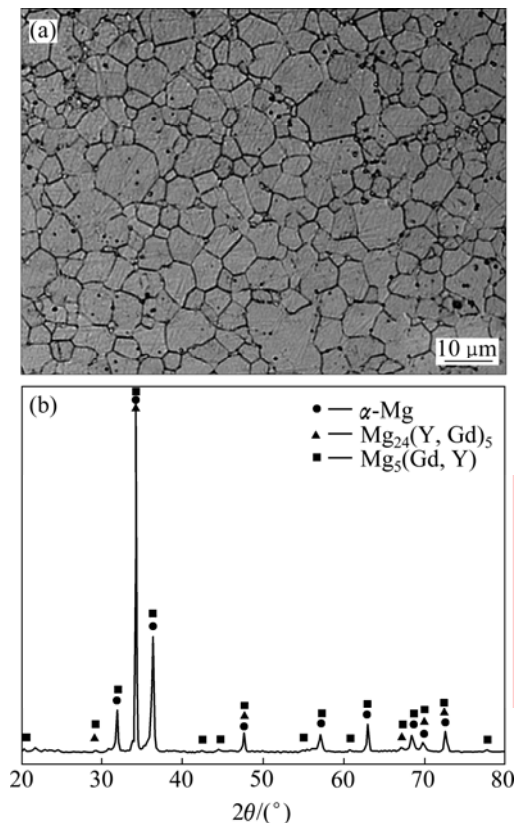


Fig.2 Microstructure(a) and XRD pattern(b) of tested alloy aged at 498 K for 12 h

4 Discussion

4.1 Effects of primary phases on fracture behavior

As mentioned above, primary phases with high-

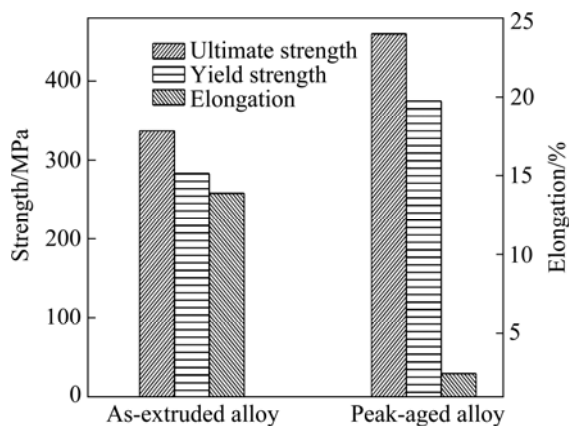


Fig.3 Tensile properties for as-extruded alloy and alloy aged at 498 K for 12 h and RT

melting point exist in the alloy. Fig.5(a) shows the enrichment region of primary phases for as-extruded alloy. Because of its brittleness, the phases are easily broken during the deformation (shown by arrow 1). The fracture can be attributed to the broken phases on the fracture surface, as shown by arrow 2. When the load reaches the maximum value, the necking happens in local region. The three-direction stress occurs in the necking zone, and the maximum stress is in axial direction. Because of the effects of three-direction stress, plastic deformation is hard to happen, which causes the brittle phases to be broken and divorced from the matrix. Therefore, lots of microvoids form. Because of the formation of microcracks from the aggregation and combination of microvoids, the alloy is ruptured

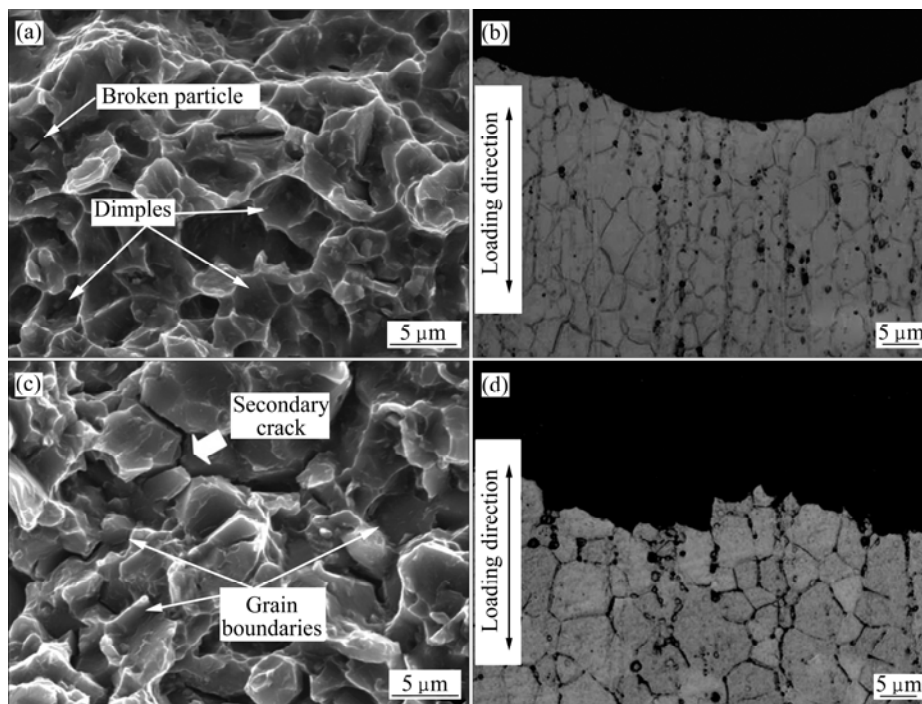


Fig.4 SEM images of fracture surfaces(a), (c) and cross-sections near fracture surfaces(b), (d) for as-extruded alloy((a) and (b)) and alloy aged at 498 K for 12 h((c) and (d)), respectively

eventually. It is identified that the fracture mechanism of as-extruded alloy is microvoid accumulation fracture.

Although the same phenomenon is found in peak-aged alloy, as shown in Fig.5(b), it is not the main factor leading to the rupture with considering the precipitation behavior. The details will be discussed in next section.

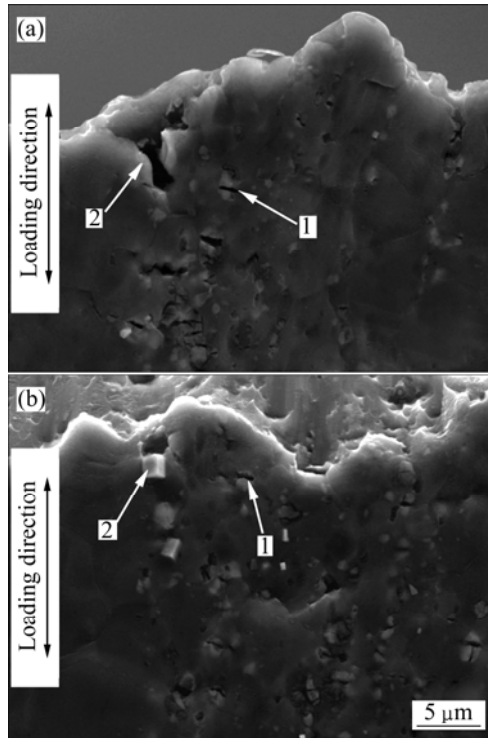


Fig.5 SEM images of cross-sectional morphologies near fracture surfaces: (a) As-extruded alloy; (b) Alloy aged at 498 K for 12 h

4.2 Effects of precipitate phases on fracture behavior

For the aged alloy, the precipitated phases inside grains and at the grain boundaries form during the aging process. Fig.6 shows the TEM images of the precipitates. From Fig.6(a) which is observed from $[0001]_{\alpha}$ direction, it can be seen that the shape of the precipitate looks like bamboo leaf with an average width of about 50 nm and a thickness of about 10 nm; while it looks like needle shape as shown in Fig.6(b) which is observed from $[10\bar{1}0]_{\alpha}$ direction. The TEM images indicate that the morphology of the precipitate is cylindrical; it is elongated to c axis of the matrix; and the cross sectional shape is ellipsoidal[15]. The plate-shaped precipitates, which form on the prismatic planes of the matrix in a dense triangular arrangement, are vertical to basal plane of α -Mg and very thermally stable at high temperature[16–18], providing the most effective block for slipping of dislocation[19–20]. The grain boundaries are weakened as compared with precipitation-hardened matrix.

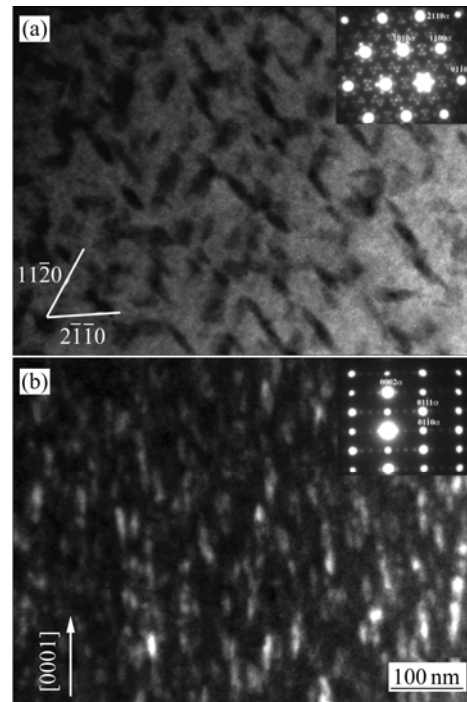


Fig.6 TEM images of testing alloy aged at 498 K for 12 h: (a) Bright field image along $[0001]_{\alpha}$ zone axis; (b) Park field image along $[10\bar{1}0]_{\alpha}$ zone axis

The TEM observation of the grain boundary precipitates (GBP) is shown in Fig.7. It can be seen that the granular precipitates distribute discontinuously along the grain boundary, and the space of precipitates is very small. As reported by ZHENG et al[14], the precipitate phases along the grain boundaries are equilibrium β phases.

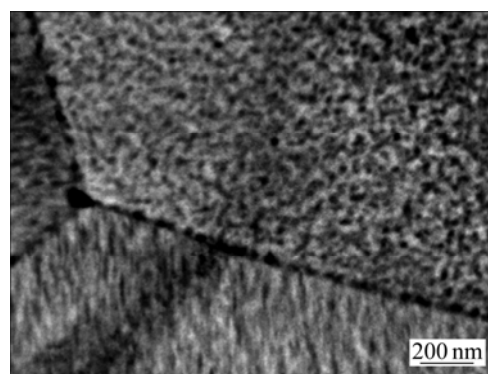


Fig.7 TEM image of precipitate phases at grain boundaries in 498 K aged alloy

Because of the presence of GBP and narrow space between the precipitates, stress concentration occurs at grain boundaries. The stress concentration subsequently promotes the growth of microvoids nucleated by the interfaces debonding between GBP and matrix under a critical stress, as shown in Fig.8 (marked with circle). Microcracks are formed by the coalescence of the

microvoids. Once the microcrack nucleates at grain boundary, it propagates along the grain boundary, as shown in Fig.8 by arrows. Such a decohesive process is typical in aged alloy with the microstructure consisting of fine precipitates (named β' phase) in the matrix and smaller precipitates on grain boundaries as well as narrow space between the precipitates[14]. It seems that the cohesive strength of the grain boundary is reduced by the existence of GBP and narrow space between the precipitates. On the other hand, the stress concentration at grain boundaries cannot be effectively relaxed by the narrow space. These factors cause the occurrence of brittle intergranular fracture.

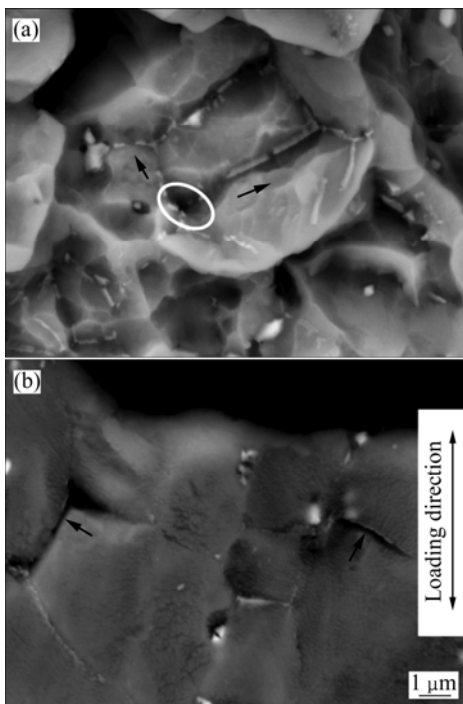


Fig.8 BEI morphologies of precipitate phases at grain boundaries for aged alloy: (a) Fracture surface; (b) Cross-section near fracture surface

5 Conclusions

1) The fracture mode for Mg-10Gd-3Y-0.6Zr alloy can be described as ductile transgranular fracture in as-extruded condition and intergranular fracture in peak-aged condition.

2) The ductile transgranular fracture for as-extruded alloy occurs because of the formation and transgranular propagation of the microcrack from the broken primary phases. It is identified that the fracture mechanism is microvoid accumulation fracture.

3) As the collaboration effects of precipitates inside grains and at the grain boundaries have the tendency to reduce the cohesive strength of the grain boundaries, and make the grain boundaries the favorable path for crack propagation, the intergranular fracture occurs in peak-

aged condition.

References

- [1] MORDIKE B L, EBERT T. Magnesium: Properties-applications-potential [J]. *Mater Sci Eng A*, 2001, 302: 37–45.
- [2] XU D K, LIU L, XU Y B, HAN E H. The effect of precipitates on the mechanical properties of ZK60-Y alloy [J]. *Mater Sci Eng A*, 2006, 420: 322–332.
- [3] LI Wen-xian, TIAN Rong-zhang. Magnesium and magnesium alloys [M]. Changsha: Central South University Press, 2005: 358–363. (in Chinese)
- [4] NIE J F, GAO X, ZHU S M. Enhanced age hardening response and creep resistance of Mg-Gd alloys containing Zn [J]. *Scripta Mater*, 2005, 53: 1049–1053.
- [5] PENG Q M, WU Y M, FANG D Q, MENG J, WANG L M. Microstructure and properties of Mg-7Gd alloy containing Y [J]. *Journal of Alloys and Compounds*, 2007, 430: 252–256.
- [6] WANG Y X, GUAN S K, ZENG X Q, DING W J. Effects of RE on the microstructure and mechanical properties of Mg-8Zn-4Al magnesium alloy [J]. *Mater Sci Eng A*, 2006, 416: 109–118.
- [7] ANYANWU I A, KAMADO S, KOJIMA Y. Aging characteristics and high temperature tensile properties of Mg-Gd-Y-Zr alloys [J]. *Mater Trans*, 2001, 42(7): 1206–1211.
- [8] MORDIKE B L. Creep-resistant magnesium alloys [J]. *Mater Sci Eng A*, 2002, 324: 103–112.
- [9] GAO Yan, WANG Qu-dong, GU Jin-hai, ZHAO Yang, TONG Yan, JUNYA K. Effects of heat treatments on microstructure and mechanical properties of Mg-15Gd-5Y-0.5Zr alloy [J]. *Journal of Rare Earths*, 2008, 26(2): 298–302.
- [10] HE S M, ZENG X Q, PENG L M, GAO X, NIE J F, DING W J. Precipitation in a Mg-10Gd-3Y-0.4Zr (wt. %) alloy during isothermal ageing at 250 °C [J]. *Journal of Alloys and Compounds*, 2006, 421: 309–313.
- [11] WANG J, MENG J, ZHANG D P, TANG D X. Effect of Y for enhanced age hardening response and mechanical properties of Mg-Gd-Y-Zr alloys [J]. *Mater Sci Eng A*, 2007, 456: 78–84.
- [12] FU P H, PENG L M, JIANG H Y, ZHANG Z Y, ZHAI C Q. Fracture behavior and mechanical properties of Mg-4Y-2Nd-1Gd-0.4Zr (wt. %) alloy at room temperature [J]. *Mater Sci Eng A*, 2008, 486: 572–579.
- [13] KOBAYASHI T. Strength and fracture of aluminum alloys [J]. *Mater Sci Eng A*, 2000, 286: 333–341.
- [14] ZHENG K Y, DONG J, ZENG X Q, DING W J. Effect of precipitation aging on the fracture behavior of Mg-11Gd-2Nd-0.4Zr cast alloy [J]. *Materials Characterization*, 2008, 59: 857–862.
- [15] HONMA T, OHKUBO T, HONO K, KAMADO S. Chemistry of nanoscale precipitates in Mg-2.1Gd-0.6Y-0.2Zr (at. %) alloy investigated by the atom probe technique [J]. *Mater Sci Eng A*, 2005, 395: 301–306.
- [16] HE S M, ZENG X Q, PENG L M, GAO X, NIE J F, DING W J. Microstructure and strengthening mechanism of high strength Mg-10Gd-2Y-0.5Zr alloy [J]. *Journal of Alloys and Compounds*, 2007, 427: 316–323.
- [17] ROKHLIN L L, NIKITINA N I. Recovery after ageing of Mg-Y and Mg-Gd alloys [J]. *Journal of Alloys and Compounds*, 1998, 279: 166–170.
- [18] APPS P J, KARIMZADEH H, KING J F, LORIMER G W. Precipitation reactions in magnesium-rare earth alloys containing yttrium, gadolinium or dysprosium [J]. *Scripta Mater*, 2003, 48: 1023–1028.
- [19] NIE J F. Effects of precipitate shape and orientation on dispersion strengthening in magnesium alloys [J]. *Scripta Mater*, 2003, 48: 1009–1015.
- [20] ANTION C, DONNADIEU P, PERRARD F, DESCHAMPS A, TASSIN C, PISCH A. Hardening precipitation in a Mg-4Y-3RE alloy [J]. *Acta Mater*, 2003, 51: 5335–5348.

(Edited by CHEN Wei-ping)